
SEPARATE CHEMICAL FREEZE-OUTS OF STRANGE AND NON-STRANGE HADRONS AND PROBLEM OF RESIDUAL CHEMICAL NON-EQUILIBRIUM OF STRANGENESS IN RELATIVISTIC HEAVY ION COLLISIONS

K.A. BUGAEV,¹ D.R. OLIINYCHENKO,^{1,2} V.V. SAGUN,¹ A.I. IVANYTSKYI,¹ J. CLEYMANS,³ E.S. MIRONCHUK,⁴ E.G. NIKONOV,⁵ A.V. TARANENKO,⁶ G.M. ZINOVJEV¹

¹**Bogolyubov Institute for Theoretical Physics, Nat. Acad. of Sci. of Ukraine**
(14b, Metrolohichna Str., Kyiv 03680, Ukraine; e-mail: bugaev@th.physik.uni-frankfurt.de)

²**FIAS,Goethe-University,**
(Ruth-Moufang Str. 1, 60438 Frankfurt upon Main, Germany; e-mail: dimafopf@gmail.com)

³**Department of Physics, University of Cape Town**
(Rondebosch 7701, South Africa; e-mail: jean.cleymans@uct.ac.za)

⁴**Moscow Institute of Physics and Technology**
(Dolgoprudnyi, 141700 Moscow Region, Russia; e-mail:)

⁵**Laboratory for Information Technologies, JINR**
(141980 Dubna, Russia; e-mail: e.nikonov@jinr.ru)

⁶**National Research Nuclear University “MEPhI” (Moscow Engineering Physics Institute)**
(Kashirskoe Shosse 31, 115409 Moscow, Russia; e-mail:)

PACS 25.75.-q, 25.75.Nq

arXiv:1610.03269v1 [nucl-th] 11 Oct 2016

We present an elaborate version of the hadron resonance gas model with the combined treatment of separate chemical freeze-outs for strange and non-strange hadrons and with an additional γ_s factor which accounts for the remaining strange particle non-equilibration. Within suggested approach the parameters of two chemical freeze-outs are connected by the conservation laws of entropy, baryonic charge, third isospin projection and strangeness. The developed model enables us to perform a high-quality fit of the hadron multiplicity ratios measured at AGS, SPS and RHIC with $\chi^2/dof \simeq 0.93$. A special attention is paid to a successful description of the Strangeness Horn. The well-known problem of selective suppression of $\bar{\Lambda}$ and $\bar{\Xi}$ hyperons is also discussed. The main result is that for all collision energies the γ_s factor is about 1 within the error bars, except for the center of mass collision energy 7.6 GeV at which we find about 20% enhancement of strangeness. Also we confirm an existence of strong jumps in pressure, temperature and effective number of degrees of freedom at the stage of strange particle chemical freeze-out, when the center of mass collision energy changes from 4.3 to 4.9 GeV. We argue that these irregularities may signal about the quark-hadron phase transition.

1. Introduction

Relativistic nucleus-nucleus (A+A) collisions provide us with experimental information about the phase diagram of quantum chromodynamics (QCD) and the strongly interacting matter properties. The last stage of such collisions is traditionally analyzed within the statistical approach which gives us an excellent opportunity to reveal the parameters of chemical freeze-out. This approach is based on the assumption of the thermal equilibrium existence during the last stage of A+A reaction. Such an equilibrium can be reached due to intensive particle scattering. The stage of the system evolution when the inelastic reactions between hadrons stop is referred to as a chemical freeze-out (FO). Particle yields are determined by the parameters of FO, namely by chemical potentials and temperature. This general picture is a basis of the Hadron Resonance Gas Model (HRGM) [1] which is the most successful one in describing the hadronic yields measured in heavy-ion experiments for

energies from AGS to LHC. Despite a significant success of the HRGM, in the experimental data analysis there are a few unresolved problems. In general they are related to the description of hadron yields which contain (anti)strange quarks. Thus, the energy dependence of K^+/π^+ and Λ/π^- ratios remained out of high quality description for almost a decade. Excess of strange hadrons yields within the HRGM led physical community to ponder over strangeness suppression in heavy ion collisions. The first receipt to resolve this problem was to introduce the strangeness suppression factor γ_s which should be fitted in order to describe the experimental data [2]. However, such an approach is not supported by any underlying physical model and the physical meaning of γ_s remains unclear [1,3–8]. In addition the strangeness suppression approach in its original form does not contain a hard-core repulsion between hadrons, while the latter is an important feature of the HRGM. A significant role of the hard-core repulsion was demonstrated once more in Ref. [5] where the global fit of hadron yield ratios was essentially improved (to $\chi^2/dof \simeq 1.16$) compared to all previous analyses.

The most advanced way to account for the hard-core repulsion between hadrons is to consider a hadron gas as a multi-component mixture of particles with different hard-core radii [4–7, 9, 10]. Within this approach all baryons and mesons except for the kaons and the pions are endowed by the common hard-core radii R_b and R_m , respectively. At the same time the kaon and the pion radii R_K and R_π are fitted independently in order to provide the best description of K^+/π^+ ratio [5]. This is an important finding since the non-monotonic energy dependence of K^+/π^+ ratio may indicate some qualitative changes of the system properties and may serve as a signal of the deconfinement onset. This is a reason why such a ratio known as the Strangeness Horn is of a special interest. Note, that the multi-component approach substantially increased the Strangeness Horn description quality, without spoiling the other ratios including Λ/π^- one. However, even this advanced approach does not reproduce the topmost point of the Strangeness Horn indicating that the data description is still not ideal. In order to resolve this problem in Ref. [7] the γ_s factor was considered as a free parameter within the HRGM with multi-component repulsion. Although the γ_s data fit sizably improves the quality of Strangeness Horn description, it does not seem to be useful for the description of other hadron multiplicities [7, 9]. Furthermore, in contrast to the claims established on the low-quality fit [11], at low energies it was found [7] that within the error bars in heavy ion collisions there is an enhance-

ment of strangeness, i.e. $\gamma_s > 1$, and not a suppression. The strangeness enhancement was confirmed very recently [12] by the high quality fit of the available data within the multicomponent HRGM in which the hard-core radius of Λ (anti)hyperon was considered as a global fitting parameter in addition to the set of hard-core radii used in [4–7, 9].

However, the effect of apparent strangeness non-equilibration can be more successfully explained by the hypothesis of separate chemical FO for all strange hadrons. Since all the hadrons made of u and d quarks are under thermal equilibration whereas the hadrons containing s quark are not, then it is reasonable to assume two different FOs for these two kinds of particles. Following this conclusion in Ref. [7, 8] a separate strangeness FO (SFO) was introduced. Note, that according to [7] both FO and SFO parameters are connected by the conservation laws of entropy, baryonic charge and isospin projection, while the net strangeness is explicitly set to zero at FO and at SFO. These conservation laws are crucial elements of the concept of separate SFO developed in [7] which allows one to essentially reduce the number of independent fitting parameters. Another principal element that differs the HRGM of [7, 9] from the ideal gas treatment used in [8, 13] is the presence of multi-component hard-core repulsion.

Using the HRGM of [7] it was possible to successfully describe all hadron multiplicities measured in A+A collisions at AGS, SPS and RHIC energies with $\chi^2/dof \simeq 1.06$. The concept of separate SFO led to a systematic improvement of all experimental data description. However, the topmost point of the Strangeness Horn again was not fitted even within the experimental error, although the general description of K^+/π^+ ratio energy dependence was rather good except for the upper point.

Since an introduction of the γ_s factor demonstrated a remarkable description of all points of the Strangeness Horn, whereas the separate SFO led to a systematic improvement of all hadron yields description, we decided to combine these elements in order to describe an experimental data with the highest possible quality. In this way we would like to examine the problem whether the concept of separate SFO is able to completely explain a possible non-equilibrium of strange charge and whether on top of the SFO there exist a necessity to employ the γ_s factor in statistical approach. Note that from the academic point of view the problem of residual strangeness non-equilibration, i.e. the question whether the strange charge is or is not in full chemical equilibrium, is of principal importance. This ambitious task is the main goal of the present paper. Evidently, the best tool for such

a purpose is the most successful version of the HRGM, i.e. the HRGM with the multi-component hadronic repulsion and a separate SFO. As it will be shown below, such an approach allows us to describe 111 independent hadron yield ratios measured for 14 values of the center of mass collision energy $\sqrt{s_{NN}}$ in the interval from 2.7 GeV to 200 GeV with very high quality.

The paper is organized as follows. The basic features of the developed model are outlined in Section 2, while the fitting procedure of the present model is outlined in Section 3. The main obtained results are compared with the other models in Section 4. In Section 5 we discuss in detail the new fit of hadronic multiplicity ratios with two chemical freeze-outs and γ_s factor, while Section 6 contains our conclusions.

2. Model description

In what follows we treat a hadronic system as a multi-component Boltzmann gas of hard spheres. The effects of quantum statistics are negligible for typical temperatures of the hadronic gas whereas the hard-core repulsion between the particles significantly affects a corresponding equation of state [5, 10]. The present model is dealing with the Grand Canonical treatment. Hence a thermodynamic state of system under consideration is fixed by the volume V , the temperature T , the baryonic chemical potential μ_B , the strange chemical potential μ_S and the chemical potential of the isospin third component μ_{I3} . These parameters control the pressure p of the system. In addition they define the densities ρ_i^K of corresponding charges Q_i^K ($K \in \{B, S, I3\}$). Introducing the symmetric matrix of the second virial coefficients $b_{ij} = \frac{2\pi}{3}(R_i + R_j)^3$, we can obtain the parametric equation of state of the present model in a compact form

$$p = \sum_{i=1}^N p_i, \quad \rho_i^K = \frac{Q_i^K p_i}{T + \frac{\sum_{j,l} p_j b_{jl} p_l}{p}}, \quad (1)$$

using the partial pressure p_i of i -th sort of particles. The equation of state is written in terms of the solutions p_i of the following system

$$p_i = T \phi_i(T) \exp \left[\frac{\mu_i - 2 \sum_j p_j b_{ji} + \sum_{j,l} p_j b_{jl} p_l / p}{T} \right], \quad (2)$$

$$\phi_i(T) = \frac{g_i}{(2\pi)^3} \int \exp \left(-\frac{\sqrt{k^2 + m_i^2}}{T} \right) d^3k. \quad (3)$$

Each i^{th} sort is characterized by its full chemical potential $\mu_i = Q_i^B \mu_B + Q_i^S \mu_S + Q_i^{I3} \mu_{I3}$, mass m_i and degeneracy g_i . The function $\phi_i(T)$ denotes the corresponding

particle thermal density in case of ideal gas. The obtained model parameters for two freeze-outs and their dependence on the collision energy are discussed in the next section. They are obtained for the following values of hard-core radii which were determined earlier in [5, 7]: $R_\pi = 0.1$ fm for pions, $R_K = 0.38$ fm for kaons, $R_m = 0.4$ for all other mesons and $R_b = 0.2$ fm for all baryons.

In order to account for the possible strangeness non-equilibration we introduce the γ_s factor in a conventional way by replacing ϕ_i in Eq. (2) as

$$\phi_i(T) \rightarrow \phi_i(T) \gamma_s^{s_i}, \quad (4)$$

where s_i is a number of strange valence quarks plus number of strange valence anti-quarks.

The principal difference of the present model from the traditional approaches is that we employ an independent chemical FO of strange particles. Let us consider this in some detail. The independent freeze-out of strangeness means that inelastic reactions (except for the decays) with hadrons made of s quarks are switched off at the temperature T_{SFO} , the baryonic chemical potential $\mu_{B_{SFO}}$, the strange chemical potential $\mu_{S_{SFO}}$, the isospin third projection chemical potential $\mu_{I3_{SFO}}$ and the three-dimensional emission volume V_{SFO} . In general case these parameters of SFO do not coincide with the temperature T_{FO} , the chemical potentials $\mu_{B_{FO}}$, $\mu_{S_{FO}}$, $\mu_{I3_{FO}}$ and the volume V_{FO} which characterize the freeze-out of non-strange hadrons. The particle yields are given by the charge density ρ_i^K in (1) and the corresponding volume at FO and at SFO.

At the first glance a model with independent SFO contains four extra fitting parameters for each energy value compared to the traditional approach (temperature, three chemical potentials and the volume at SFO instead of strangeness suppression/enhancement factor γ_s). However, this is not the case due to the conservation laws. Indeed, since the entropy, the baryonic charge and the isospin third projection are conserved, then the parameters of FO and SFO are connected by the following equations

$$s_{FO} V_{FO} = s_{SFO} V_{SFO}, \quad (5)$$

$$\rho_{FO}^B V_{FO} = \rho_{SFO}^B V_{SFO}, \quad (6)$$

$$\rho_{FO}^{I3} V_{FO} = \rho_{SFO}^{I3} V_{SFO}, \quad (7)$$

where the entropy density $s_A = \frac{\partial p}{\partial T}|_A$, the density of baryonic charge $\rho_A^B = \frac{\partial p}{\partial \mu^B}|_A$ and the density of the isospin third projection $\rho_A^{I3} = \frac{\partial p}{\partial \mu^{I3}}|_A$ are found from the usual thermodynamic identities at the SFO ($A=SFO$) or at FO ($A=FO$).

The effective volumes can be excluded, if these equations are rewritten as

$$\frac{s}{\rho^B} \Big|_{\text{FO}} = \frac{s}{\rho^B} \Big|_{\text{SFO}}, \quad \frac{\rho^B}{\rho^{I_3}} \Big|_{\text{FO}} = \frac{\rho^B}{\rho^{I_3}} \Big|_{\text{SFO}}. \quad (8)$$

Thus, the baryonic $\mu_{B\text{SFO}}$ and the isospin third projection $\mu_{I_3\text{SFO}}$ chemical potentials at SFO are now defined by Eqs. (8). Note, that the strange chemical potentials $\mu_{S\text{FO}}$ and $\mu_{S\text{SFO}}$ are found from the condition of vanishing net strangeness at FO and SFO, respectively. Therefore, the concept of independent SFO leads to an appearance of one independently fitting parameter T_{SFO} . Hence, the independent fitting parameters are the following: the baryonic chemical potential μ_B , the chemical potential of the third projection of isospin μ_{I_3} , the chemical freeze-out temperature for strange hadrons T_{SFO} , the chemical freeze-out temperature for all non-strange hadrons T_{FO} and the γ_s factor (i.e. 5 fitting parameters for each collision energy).

An inclusion of the width Γ_i of hadronic states is an important element of the present model. It is due to the fact that the thermodynamic properties of the hadronic system are sensitive to the width [5, 7, 14]. In order to account for the finite width of resonances we perform the usual modification of the thermal particle density ϕ_i . Namely, we convolute the Boltzmann exponent under the integral over momentum with the normalized Breit-Wigner mass distribution. As a result, the modified thermal particle density of i^{th} sort hadron acquires the form

$$\int \exp\left(-\frac{\sqrt{k^2 + m_i^2}}{T}\right) d^3k \rightarrow \frac{\int_{M_0}^{\infty} \frac{dx}{(x-m_i)^2 + \Gamma_i^2/4} \int \exp\left(-\frac{\sqrt{k^2 + x^2}}{T}\right) d^3k}{\int_{M_0}^{\infty} \frac{dx}{(x-m_i)^2 + \Gamma_i^2/4}}. \quad (9)$$

Here m_i denotes the mean mass of hadron and M_0 stands for the threshold in the dominant decay channel. The main advantages of this approximation is a simplicity of its realization and a clear way to account for the finite width of hadrons. It is appropriate here to mention that one could use other prescriptions to account for the width of resonances. However, in a recent work [14] it was shown the Breit-Wigner prescription (9) can provide somewhat better (about 20%) quality of the fit than the Gaussian attenuation of resonance mass and essentially better one compared to the case without accounting for the width. At the same time in [14] it was found that within the error bars such FO parameters as temperature, chemical potentials and γ_s factor are the same

for different prescriptions of resonance width accounting. Clearly, it is reasonable to expect that other physically motivated ways to account for the resonance width should give similar results. Therefore, in this work we employed the prescription (9), which provides the better description of the data.

The observed hadronic multiplicities contain the thermal and decay contributions. For example, a large part of pions is produced by the decays of heavier hadrons. Therefore, the total multiplicity is obtained as a sum of thermal and decay multiplicities, exactly as it is done in a conventional model. However, writing the formula for final particle densities, we have to take into account that the FO and SFO volumes can be different:

$$\frac{N^{\text{fin}}(X)}{V_{\text{FO}}} = \sum_{Y \in \text{FO}} BR(Y \rightarrow X) \rho^{\text{th}}(Y) + \sum_{Y \in \text{SFO}} BR(Y \rightarrow X) \rho^{\text{th}}(Y) \frac{V_{\text{SFO}}}{V_{\text{FO}}}. \quad (10)$$

Here the first term on the right hand side is due to decays after FO whereas the second one accounts for the strange resonances decayed after SFO. The factor $V_{\text{SFO}}/V_{\text{FO}}$ can be replaced by $\rho_{\text{FO}}^B/\rho_{\text{SFO}}^B$ due to baryonic charge conservation. $BR(Y \rightarrow X)$ denotes the branching ratio of the Y-th hadron decay into the X-th hadron, with the definition $BR(X \rightarrow X) = 1$ used for the sake of convenience. The input parameters of the present model (masses m_i , widths Γ_i , degeneracies g_i and branching ratios of all strong decays) were taken from the particle tables of the thermodynamical code THERMUS [15].

3. Fitting Procedures

Data sets. The present model is applied to fit the data. We take the ratios of particle multiplicities at midrapidity as the data points. In contrast to fitting multiplicities themselves such an approach allows us to cancel the possible experimental biases. In this paper we use the data set almost identical to Ref. [7]. At the AGS energies ($\sqrt{s_{NN}} = 2.7 - 4.9$ AGeV or $E_{\text{lab}} = 2 - 10.7$ AGeV) the data are available with a good energy resolution above 2 AGeV. However, for the beam energies 2, 4, 6 and 8 AGeV only a few data points are available. They corresponds to the yields for pions [16, 17], for protons [18, 19], for kaons [17] (except for 2 AGeV). The integrated over 4π data are also available for Λ hyperons [20] and for Ξ^- hyperons (for 6 AGeV only) [22]. However, as was argued in Ref. [1], the data for Λ and Ξ^- should be recalculated for midrapidity. Therefore, instead of raw experimental data we used the corrected values from

Table 1. The fit results of different versions of the HRGM are compared for 14 values of the center of mass collision energies: the column χ_1^2 corresponds to a single FO model of [5]; the column χ_2^2 is found for the SFO with $\gamma_s = 1$ [7]; the column χ_3^2 corresponds to the SFO+ γ_s fit with added data points for $N_{rat} \leq 5$ while the column χ_4^2 is obtained by the direct SFO $\oplus\gamma_S$ fit. N_{rat} indicates the available number of independent hadronic ratios at given center of mass collision energy $\sqrt{s_{NN}}$. In the row Sum we list the sum of i -th column, while in the bottom row the number of degrees of freedom of each HRGM version is shown (for more details see the text).

$\sqrt{s_{NN}}$ (GeV)	χ_1^2 FO	N_{rat}	χ_2^2 SFO	χ_3^2 SFO+ γ_S	χ_4^2 SFO $\oplus\gamma_S$
2.7	0.62	4	0.62	0.62	$1.3 \cdot 10^{-5}$
3.3	0.17	5	0.08	0.08	$3.4 \cdot 10^{-9}$
3.8	0.56	5	0.03	0.03	0.03
4.3	0.35	5	0.26	0.26	0.21
4.9	0.55	8	0.55	0.40	0.40
6.3	7.91	9	2.88	2.45	2.45
7.6	17.5	10	16.6	5.9	5.9
8.8	7.9	11	7.85	7.56	7.56
9.2	0.16	5	0.15	0.03	$1.3 \cdot 10^{-7}$
12	17.3	10	11.9	9.57	9.57
17	14.7	13	7.39	7.38	7.38
62.4	0.4	5	0.09	0.03	0.03
130	5	11	4.62	4.32	4.32
200	7.4	10	5.49	5.09	5.09
Sum	80.5	111	58.5	43.72	42.9
Dof	69	N/A	55	47	41

[1]. Next comes the data set at the highest AGS energy ($\sqrt{s_{NN}} = 4.9$ AGeV or $E_{lab} = 10.7$ AGeV). Similarly to [5], here we analyzed only the NA49 mid-rapidity data [23–28]. Since the RHIC high energy data of different collaborations agree with each other, we analyzed the STAR results for $\sqrt{s_{NN}} = 9.2$ GeV [29], $\sqrt{s_{NN}} = 62.4$ GeV [30], $\sqrt{s_{NN}} = 130$ GeV [31–34] and $\sqrt{s_{NN}} = 200$ GeV [34–36].

Combined fit with SFO and γ_s factor. A comprehensive data analysis [7] performed recently for two alternative approaches, i.e the first one with γ_s as a free parameter and the second one with separate FO and SFO, showed the advantages and disadvantages of both methods. Thus, the γ_s fit provides one with an opportunity to noticeably improve the Strangeness Horn description with $\chi^2/dof = 3.3/14$, comparably to the previous result $\chi^2/dof = 7.5/14$ [5], but there are only slight improvements of the ratios with strange baryons (global $\chi^2/dof : 1.16 \rightarrow 1.15$). The obtained results for the SFO approach demonstrate a high fit quality for the most problematic ratios for the HRGM, especially

for \bar{p}/π^- , $\bar{\Lambda}/\Lambda$, $\bar{\Xi}^-/\Xi^-$ and $\bar{\Omega}/\Omega$. Although the overall $\chi^2/dof \simeq 1.06$ is notably better than with the γ_s factor [5, 7], but the description of the Horn’s highest point got worsen. These results led us to an idea to investigate the combination of these two approaches in order to get the high-quality Strangeness Horn description without spoiling the quality of other particle ratios. However, we immediately face a mathematical problem to justify such a combined fit because at six values of the center of mass collision energies, namely $\sqrt{s_{NN}} = 2.7, 3.3, 3.8, 4.3, 9.2, 62.4$ GeV, the number of independent hadron yield ratios (4, 5, 5, 5, 5, 5, respectively) is equal or even smaller than the number of fitting parameters (see Table 1). For these energies one, of course, can treat the experimental ratios as equations and can solve them, but, unfortunately, the experimental ratios always have finite (and not small!) error bars. As a result, solving the ratios as equations with finite errors leads to rather large region of chemical FO parameters which provide a vanishing value of χ^2 and, hence, it is hard to conclude what values are the most probable ones. It seems that these difficulties prevented the authors of a recent work [13] to analyze the data at the collision energies $\sqrt{s_{NN}} \leq 4.9$ GeV within their version of SFO concept [8].

Moreover, in some cases the range of chemical FO parameters obtained by such a fit, the SFO $\oplus\gamma_S$ hereafter, is located far away from the ones found by the well established fit procedures, i.e. by the single FO model without [5] or with [7] the γ_s fit and by the SFO with $\gamma_s = 1$ [7] which provide us with very good descriptions of the data. Moreover, all these results are in a very good correspondence with each other. Therefore, the combined SFO and γ_S fit can be directly performed for the collision energies $\sqrt{s_{NN}} = 4.9, 6.3, 7.6, 8.8, 12, 17, 130, 200$ GeV only, while for other energies we have to seek for another minimization criterion.

Since the major task of the present work is to determine the residual effect of the strangeness non-equilibrium on top of the SFO, then it would be reasonable to fix the parameters of the SFO and make the γ_s fit. Unfortunately, in this case the number of degrees of freedom will be the same as for the SFO $\oplus\gamma_S$ fit, i.e. $dof = 41$, and the resulting value of χ^2/dof would not be better than the one obtained within the SFO $\oplus\gamma_S$ fit. Hence, to avoid the above mentioned problems we suggest to modify the definition of χ^2 for the six values of the collision energy which have 5 or less independent

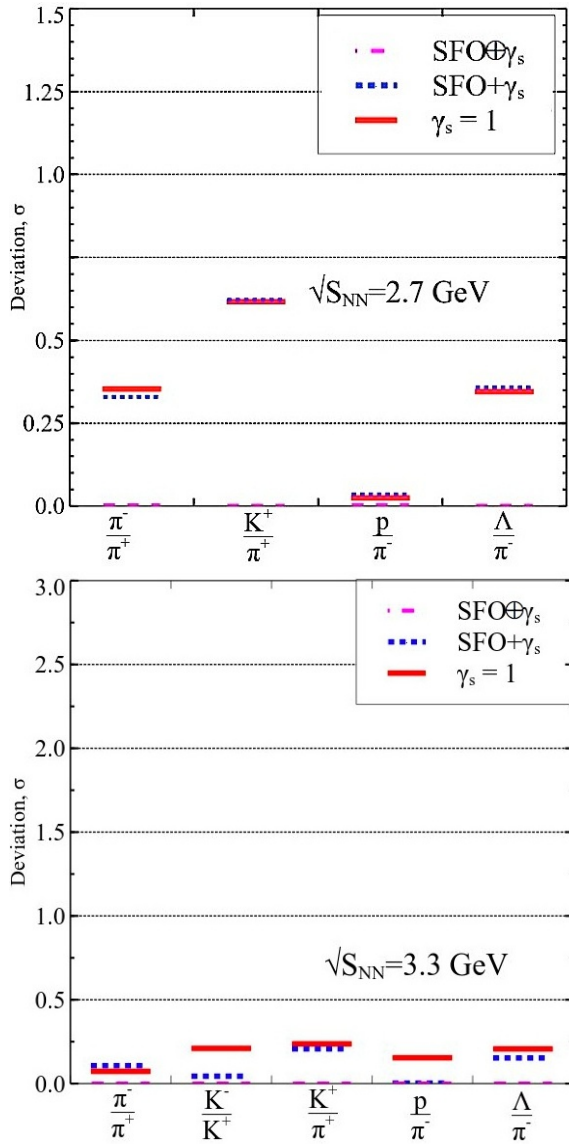


Fig. 1. (Colour on-line) Relative deviation of the theoretical description of ratios from the experimental value in units of the experimental error σ . Particle ratios vs. the modulus of relative deviation ($\frac{|r_i^{theo} - r_i^{exp}|}{\sigma_i^{exp}}$) for $\sqrt{s_{NN}} = 2.7$ and 3.3 GeV are shown. Solid lines correspond to the model with a single FO of all hadrons and $\gamma_s = 1$, the dotted lines correspond to the model SFO+ γ_s as explained in the text. The results of the SFO $\oplus\gamma_s$ model are indicated by the dashed lines.

ratios

$$\chi^2 = \sum_i \frac{(r_i^{theo} - r_i^{exp})^2}{\sigma_i^2} + \left[\frac{T_{SFO} - T_{SFO}(\gamma_s = 1)}{\sigma_T^{SFO}} \right]^2, \quad (11)$$

where r_i^{theo} and r_i^{exp} are, respectively, the theoretical and the experimental values of particle yields ratios, σ_i stands for the corresponding experimental error and a summation is performed over all experimental points which are available at the considered energy. Here σ_T^{SFO} denotes the error of the SFO temperature $T_{SFO}(\gamma_s = 1)$ which is found for each problematic energy by the SFO fit with $\gamma_s = 1$, while the chemical FO temperature of strange particles T_{SFO} is the fitting parameter.

In other words, for each energies corresponding to a set of problematic ratios we suggest to consider the SFO temperature $T_{SFO}(\gamma_s = 1)$, as an additional datum to be fitted within the combined SFO+ γ_s approach, while for other collision energies we used the standard definition $\chi^2 = \sum_i \frac{(r_i^{theo} - r_i^{exp})^2}{\sigma_i^2}$ for the combined fit. In order to distinguish this approach from the SFO $\oplus\gamma_s$ fit we refer to it as the SFO+ γ_s fit. Such a reformulation of minimization criterion for $\sqrt{s_{NN}} = 2.7, 3.3, 3.8, 4.3, 9.2, 62.4$ GeV allows us to avoid the mathematical problems of the combined SFO $\oplus\gamma_s$ fit and to simultaneously keep the temperature of strange particles T_{SFO} not far away from the SFO temperature T_{SFO} . Originally, for $\sqrt{s_{NN}} = 2.7$ we added two data points into the χ^2 definition (11) in order to have 6 data for 5 fitting parameters, but then we found that adding one data point is sufficient, since it resolves the problem.

4. Main Results

The results of the SFO+ γ_s , SFO $\oplus\gamma_s$ and SFO fits are compared for $\sqrt{s_{NN}} = 2.7$ and 3.3 GeV in Fig. 1 (for more details see also Table I). As one can see from this figure the SFO description is already very good ($\chi^2 \equiv \chi_2^2 \simeq 0.62$ in Table I) and, hence, the additional parameter γ_s cannot improve it (compare χ_3^2 and χ_2^2 in Table I), if the number of data points is equal or large than the number of fitting parameters. Thus, the mathematically justified SFO+ γ_s fitting procedure does not improve the description quality compared to the SFO fit at these collision energies and, hence, we find that $\gamma_s \simeq 1$ within the error bars. Moreover, for a completeness we used another way of fitting: first we determined the parameters of two chemical freeze-out within the SFO model with $\gamma_s = 1$ (see the χ_2^2 column in Table I), fixed the found parameters and then we performed the fitting of the γ_s parameter. It is remarkable that in this way we did not get any improvement of the fit quality compared to the SFO+ γ_s fit and got the same freeze out temperatures and chemical potentials as in the latter case not only for the problematic data points, but

within the error bars we found the same results for all other energies of collision.

The main results for the $SFO \oplus \gamma_S$ and $SFO + \gamma_s$ fits found here are as follows. Due to the problems discussed above the $SFO \oplus \gamma_S$ model does not allow us to locate the narrow region of the chemical FO parameters for the collision energies $\sqrt{s_{NN}} = 2.7, 3.3$ and 9.2 GeV, while for the energies $\sqrt{s_{NN}} = 3.8, 4.3$ and 62.4 GeV we did not find the solutions of five equations for five variables and, hence, were able to perform the usual minimization of χ^2 .

The $SFO \oplus \gamma_S$ model gives $\chi_4^2/dof = 42.96/41 \simeq 1.05$, which is only a very slight improvement compared to the previously obtained results for the SFO model $\chi_2^2/dof = 58.5/55 \simeq 1.06$. The redefinition of the χ^2 criterion (11) allows us to avoid the mathematical problems within the $SFO + \gamma_s$ model and to sizably reduce the χ^2 value per degree of freedom to $\chi_3^2/dof = 43.72/47 \simeq 0.93$. Moreover, for the problematic data at the collision energies $\sqrt{s_{NN}} = 3.8, 4.3$ and 62.4 GeV within the $SFO + \gamma_s$ model we obtained practically the same chemical FO parameters and the same quality of the fit (compare the values of χ_3^2 and χ_4^2 in Table I for these energies), as for the $SFO \oplus \gamma_S$ model, including the main conclusion that $\gamma_s \simeq 1$ (see the upper panel of Fig. 2). Such a result provides an additional justification for the χ^2 criterion redefinition (11).

Nevertheless, as one can see from Table I compared to the SFO model with $\gamma_s = 1$ (see the column with χ_2^2) the main reduction of χ^2 achieved by the γ_S parameter corresponds to $\sqrt{s_{NN}} = 7.6$ GeV, i.e this is exactly where the Strangeness Horn peak is located. Moreover, we found that the fitting results can be separated into two distinct groups: those, where $\chi^2 > 1$ and where $\chi^2 < 1$ for any of our fits. It is remarkable that neither SFO, nor γ_s fits do not move any of the points of one group to another group. If for a certain collision energy the inequality $\chi^2 > 1$ occurred, then it always holds after any of our efforts. The results obtained for the $SFO + \gamma_s$ are shown in Figs. 2–10. Note that compared to the SFO model with $\gamma_s = 1$ [7] the value of χ^2 itself for the $SFO + \gamma_S$ fit, not divided by number of degrees of freedom, has improved notably, although the deviation of the γ_s factor from 1 does not exceed 20 % even for the topmost point of the Strangeness Horn (see the upper panel of Fig. 2). Note that our results on the $SFO + \gamma_S$ model are very similar to the SFO model of Ref. [13] (just compare our Fig. 3 with Fig. 4 in [13]), although at the energies $\sqrt{s_{NN}} = 130$ GeV and $\sqrt{s_{NN}} = 200$ GeV we find that the temperature of FO is slightly higher than the temperature of SFO, while in [13] the situation

is opposite. Two possible reasons for such a difference is that in Ref. [13] the conservation laws (5)–(7) are ignored and their treatment is based on the ideal gas picture. As a result the fit quality achieved in [13] is essentially lower (see Fig. 5 in there) compared to the present work.

It is remarkable that the present rather sophisticated fit of the hadronic multiplicities confirms the recent finding on the non-smooth behavior of the function $T_{FO}(\mu_B^{FO})$ reported in [14] for the same hard-core radius of hadrons $R = 0.3$ fm. A similar change of the slope of $T_{SFO}(\mu_B^{SFO})$ occurring at the collision energy $\sqrt{s_{NN}} \simeq 4$ GeV is a new result shown in Fig. 2. Following the work [14], we parameterize $T_{FO}(\sqrt{s_{NN}})$, $T_{SFO}(\sqrt{s_{NN}})$, $\mu_B^{FO}(\sqrt{s_{NN}})$ and $\mu_B^{SFO}(\sqrt{s_{NN}})$ as

$$T = (T_1 + T_2 \sqrt{s_{NN}}) \cdot c_+(\sqrt{s_{NN}}, 4.0, 0.1) + (T_3/\sqrt{s_{NN}} + T_4) \cdot c_-(\sqrt{s_{NN}}, 4.0, 0.1), \quad (12)$$

$$\mu_B = \frac{A}{1 + B\sqrt{s_{NN}}}, \quad (13)$$

where $c_{\pm}(x, a, b)$ are the sigmoid functions

$$c_+(x, a, b) = \frac{1}{1 + e^{(x-a)/b}} = \frac{1}{2} \left(1 - \tanh \frac{x-a}{2b} \right), \quad (14)$$

$$c_-(x, a, b) = \frac{1}{1 + e^{(a-x)/b}} = \frac{1}{2} \left(1 + \tanh \frac{x-a}{2b} \right). \quad (15)$$

The main reason to employ the parameterizations (12)–(15) is a drastic change of the $\sqrt{s_{NN}}$ dependence of the function $T_{FO}(\sqrt{s_{NN}})$ in the narrow region $\sqrt{s_{NN}} \simeq 4.3 - 4.9$ GeV found in [14]. The upper panel of Fig. 3 confirms that a similar behavior of $T_{FO}(\sqrt{s_{NN}})$ and $T_{SFO}(\sqrt{s_{NN}})$ exists within the $SFO + \gamma_s$ model, although the switch value of the collision energy $\sqrt{s_{NN}} \simeq 4$ GeV is about ten percents lower than the one found for the single FO model of work [14]. The resulting curves (12) and (13) for the $SFO + \gamma_s$ model are shown in Fig. 3, whereas the corresponding parameters are give in Table 2. Using curves (12) and (13) we obtained the analytic expressions for the functions $T_{FO}(\mu_B^{FO})$ and $T_{SFO}(\mu_B^{SFO})$, which are shown in the lower panel of Fig. 2.

For a comparison in Figs. 2 and 3 we depict the parameterization of the chemical freeze out temperature ($\sqrt{s_{NN}}$ is given in GeVs)

$$T^{FO}[MeV] = \frac{T^{lim}}{1 + \exp[2.60 - \ln(\sqrt{s_{NN}})/0.45]} = T^{lim} c_-(\ln(\sqrt{s_{NN}}), 1.17, 0.45), \quad (16)$$

which together with the parameterization (13) was suggested in [1]. The parameters $T^{lim} = 164$ MeV, $A =$

Table 2. The parameters of Eqs. (12) and (13) found from fitting the values of chemical freeze out parameters of the SFO+ γ_s model.

	FO	SFO
T_1 (MeV)	-82.7	-43.9
T_2 (MeV)	48.1	34.2
T_3 (MeV)	-211.8	-254.8
T_4 (MeV)	162.8	167.2
χ^2/dof fit Eq. (12)	16/9	14.5/9
A (MeV)	1501	1525
B (GeV $^{-1}$)	0.38	0.39
χ^2/dof fit Eq. (13)	3.4/12	8.1/12

1303 MeV, $B = 0.286$ GeV $^{-1}$ were found in [3]. Although they have close values to T_4 , A and B listed in Table, only the curves $\mu_B(\sqrt{s_{NN}})$ found here and in [3] look similar (see the lower panel of Fig. 3). From the upper panel of Fig. 3 one can see that the curves (12) and (16) have rather different behavior at low and intermediate values of collision energy. As a result the functions $T_{FO}(\mu_B^{FO})$ found here and in [3] have different shapes as one can see from the lower panel of Fig. 2. We have to note that our efforts to reasonably describe the FO and SFO temperatures by the parameterization (16) were not successful and the corresponding values of χ^2/dof were almost one order of magnitude larger than the ones given in Table 2 for Eq. (12). Clearly, the found parameterizations should be considered as the predictions for the chemical FO and SFO characteristics which can be experimentally tested at the accelerators FAIR (GSI, Darmstadt) and NICA (JINR, Dubna).

In Fig. 4 we show the ratio of baryonic charge densities at SFO and at FO within the SFO+ γ_s model, which coincides with the inverse ratio of corresponding freeze-out volumes V_{FO}/V_{SFO} due to the baryonic charge conservation. From this figure one can see that visually small difference of temperatures and baryonic chemical potentials at SFO and FO leads, nevertheless, to quite sizable difference of other thermodynamic quantities. As one can see from the upper panel of Fig. 5, this is also true for the pressure existing at SFO and at FO.

Also we confirm the existence of irregularities in the FO pressure found earlier [14]. Similar irregularities we find for the SFO pressure and for the effective number of degrees of freedom for SFO, $p^{SFO}/(T^{SFO})^4$, i.e. for the ratio of SFO pressure to the fourth power of the SFO temperature. From the upper panel of Fig. 5 one can see that the largest increase of SFO pressure per increase of the center of mass energy of collision occurs at $\sqrt{s_{NN}} = 4.3 - 4.9$ GeV. In other words, for about

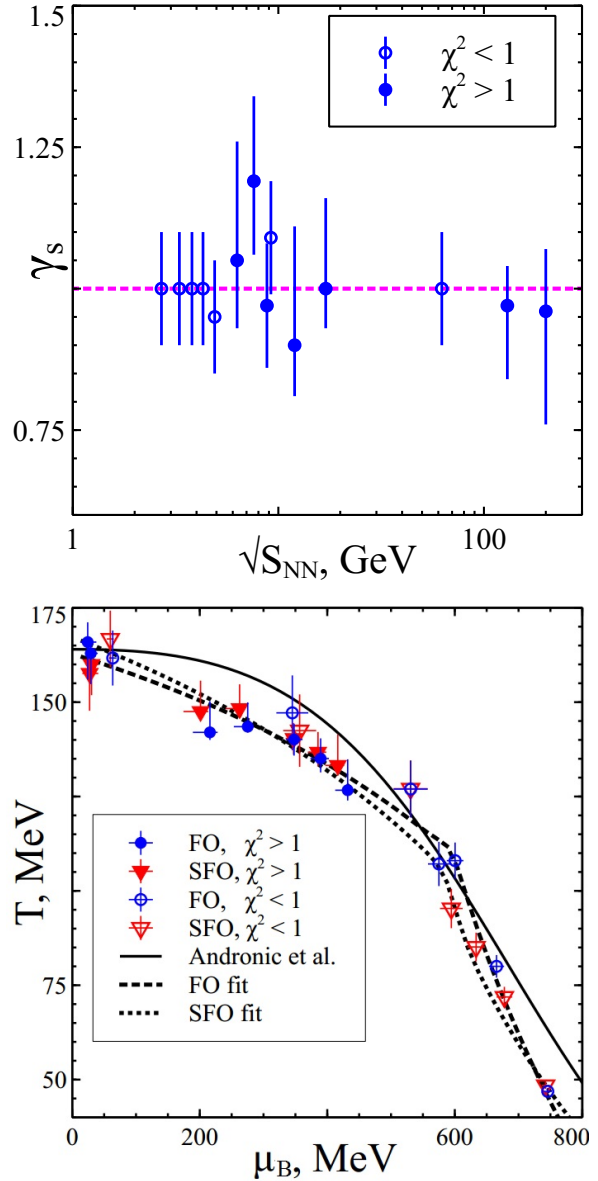


Fig. 2. (Colour on-line) **Upper panel:** $\sqrt{s_{NN}}$ dependence of the γ_s factor within the SFO+ γ_s model with two freeze-outs and the γ_s fit. **Lower panel:** Chemical freeze-outs parameters found within the SFO+ γ_s model. Baryonic chemical potential dependence of the chemical freeze-out temperature for the strange hadrons (SFO points are marked with triangles) and for the non-strange ones (FO points are marked with circles). The pairs of nearest points are connected by the isentrops $s/\rho_B = const$, on which the FO and the SFO points are located.

14% increase of $\sqrt{s_{NN}}$ the SFO pressure increases in 5.3 times and the ratio $p^{SFO}/(T^{SFO})^4$ increases on about 65%. According to the recent work [41] these and other irregularities observed at chemical FO [14] are signaling

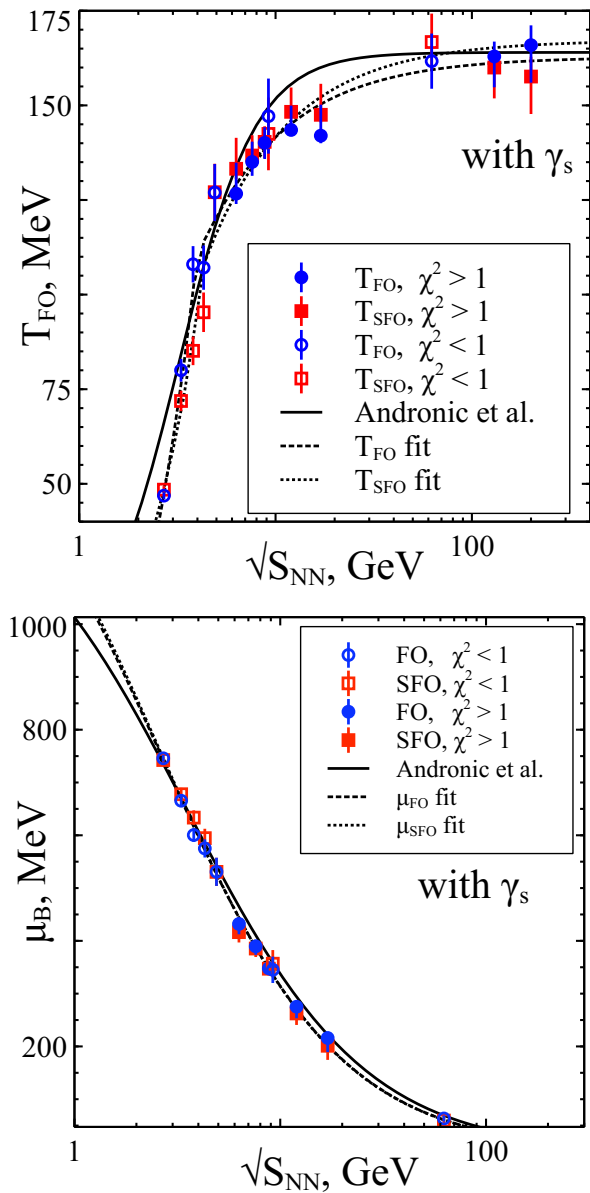


Fig. 3. (Colour on-line) The behavior of the SFO+ γ_s model parameters: the chemical freeze-out temperatures T_{FO} and T_{SFO} vs. $\sqrt{s_{NN}}$ (upper panel) and the freeze-out baryonic chemical potentials μ_B^{FO} and μ_B^{SFO} vs. $\sqrt{s_{NN}}$ (lower panel).

about the formation of the mixed quark-gluon-hadron phase and such an explanation can be experimentally verified in a few years at FAIR and NICA.

One more important finding of the present work can be seen from a comparison of the upper and lower panels of Fig. 5. Note that in contrast to the temperature or baryonic chemical potential, the pressure allows one easier to distinguish the SFO from FO. Moreover, com-

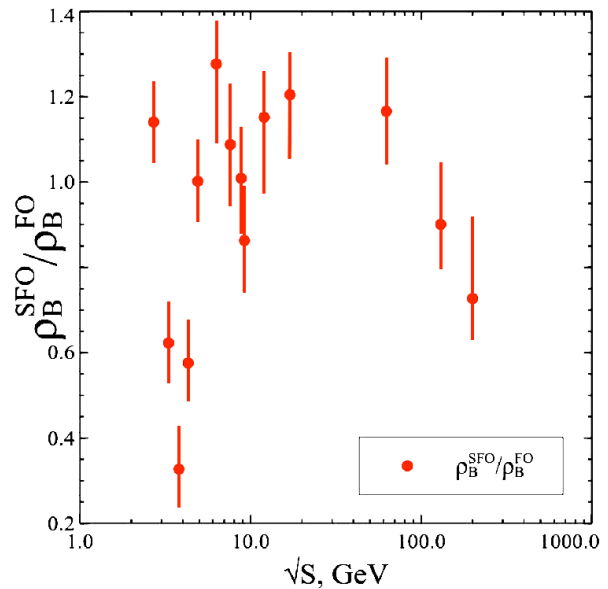


Fig. 4. (Colour on-line) $\sqrt{s_{NN}}$ dependence of the ratio of baryonic charge densities at SFO and at FO within the SFO+ γ_s model. Since the baryonic charge is conserved, then such a ratio coincides with the inverse ratio of corresponding freeze-out volumes, i.e. with V_{FO}/V_{SFO} .

paring the squares in the upper and lower panels of Fig. 5 one immediately concludes that the model of a single chemical FO [14] with the same value of hard-core radius for all hadrons describes just the SFO for all values of $\sqrt{s_{NN}}$ below 62.4 GeV. The same is true for a single FO model [5] with different hard-core radii discussed above. This peculiar result can be easily understood, if one recalls that for the most values of collision energy the number of ratios involving strange hadrons is essentially larger than the number of ratios with non-strange particles.

At the same time a single chemical FO model reproduces the FO pressure of the SFO+ γ_s model only at $\sqrt{s_{NN}} \geq 62.4$ GeV. The corresponding reasons we will discuss in the next section, while here we mention that at high RHIC energies the fit quality of all models, including the single FO one, is rather high as one can see from Table I. The main part of χ^2 at these energies is formed by poor description of K -mesons at $\sqrt{s_{NN}} = 62.4$ GeV, Λ hyperon at $\sqrt{s_{NN}} = 130$ GeV and Ω^\pm hyperons at $\sqrt{s_{NN}} = 200$ GeV.

Such a comparison of the single FO model and the SFO+ γ_s model pressures allows us to explain a cause of why in previous thorough analysis of the particle ratios within the realistic single FO model with the same hard-core radius of hadrons the main conclusion was that

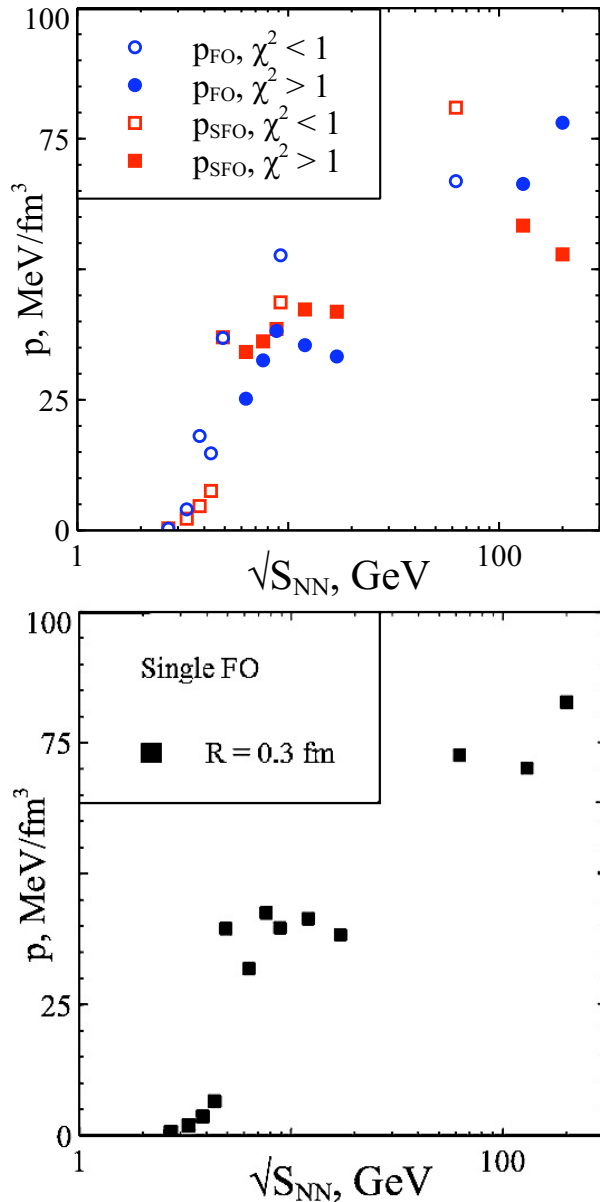


Fig. 5. (Colour on-line) $\sqrt{s_{NN}}$ dependences of the pressure at FO and SFO points found within the SFO+ γ_s model (upper panel) and within a single FO model for the same hard-core radius $R = 0.3$ fm of all hadrons [14].

there is no deviation of strange particles from chemical equilibrium for the mid-rapidity data. In other words, it is possible to naturally explain the reason of why in [1] it was found that within the error bars $\gamma_s \simeq 1$. Our direct comparison of the SFO+ γ_s model for the mid-rapidity data shows that the single FO models with the same or different hard-core hadronic radii reproduce the SFO

pressure with $\gamma_s \simeq 1$ almost at all collision energies, except for $\sqrt{s_{NN}} = 7.6$ GeV and for $\sqrt{s_{NN}} \geq 62.4$ GeV. In the former case one finds that $\gamma_s \simeq 1.19$, while in the latter case $\gamma_s \simeq 1$, but, as we discussed above, for high collision energies the pressure at FO found within the SFO+ γ_s model reproduces the single FO model pressure. Therefore, the main reason of why the chemical non-equilibrium of strange charge was not found within the single FO models is that the fitting procedure mainly described the ratios involving the strange particles and, hence, it would have been more appropriate to consider the chemical non-equilibrium of non-strange hadrons.

5. Results for Particle Ratios

The findings discussed above motivate us to study in some details what ratios and at what energies are improved. The most significant improvements correspond to the collision energies $\sqrt{s_{NN}} = 6.3, 7.6,$ and 12 GeV, that are plotted in Figs. 6 and 7. Figs. 6 and 7 demonstrate very high fit quality, especially for such traditionally problematic ratios as $K^+/\pi^+, \pi^-/\pi^+, \bar{\Lambda}/\pi^-$ and φ/K^+ , which is achieved within the SFO+ γ_s model compared to the single FO model and the SFO one. For instance, for $\sqrt{s_{NN}} = 7.6$ GeV seven ratios out of ten are improved, while for other energies the improvements are less significant. On the contrary, the particle ratios measured at $\sqrt{s_{NN}} = 17$ GeV (see Fig. 7) are improved within the SFO model, while the SFO+ γ_s fit practically does not lead to any significant improvement compared to the SFO model.

Also we found that the SFO+ γ_s fit leads to a selective improvement and to a certain degradation of the fit quality of various ratios for different collision energies. For instance, the π^-/π^+ ratio is slightly increased for $\sqrt{s_{NN}} = 6.3$ and 7.6 GeV, but the situation drastically changes for $\sqrt{s_{NN}} = 12$ GeV. The same tendency is typical for \bar{p}/p . On the contrary, for Ξ^-/Λ ratio there is a noticeably worse data description within SFO+ γ_s approach at $\sqrt{s_{NN}} = 6.3, 7.6$ GeV, but for $\sqrt{s_{NN}} = 12$ GeV the fit quality is sizably better compared to all previous approaches. Thus, within the present model we reveal a noticeable change in the trend of some ratios at $\sqrt{s_{NN}} = 7.6-12$ GeV, while at $\sqrt{s_{NN}} = 12$ GeV we do not observe any sizable improvement compared to the SFO model.

A special attention in our consideration was paid to the Strangeness Horn, i.e. to the K^+/π^+ ratio, because such a ratio is traditionally the most problematic one for the HRGM to fit it. As one can see from Fig. 8, the remarkable K^+/π^+ fit improvement for

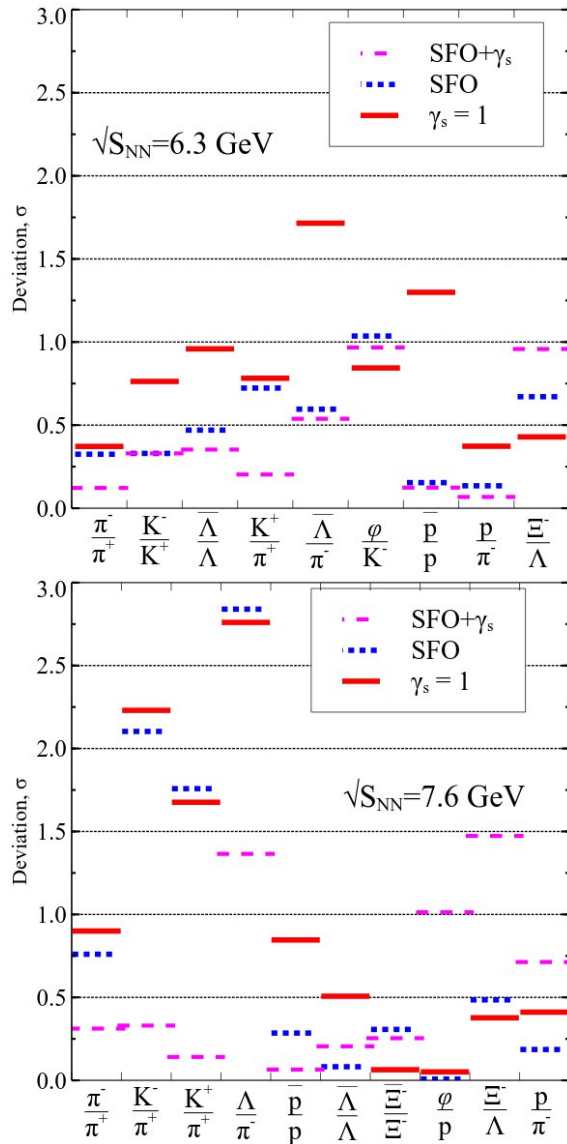


Fig. 6. (Colour on-line) Relative deviation of the theoretical description of ratios from the experimental value in units of the experimental error σ . Particle ratios vs. the modulus of relative deviation ($\frac{|r^{theor}-r^{exp}|}{\sigma^{exp}}$) for $\sqrt{s_{NN}} = 6.3$ and 7.6 GeV are shown. Solid lines correspond to the model with a single FO of all hadrons and $\gamma_s = 1$, the dotted lines correspond to the model with SFO. The results of a model with a combined fit with SFO and γ_s are indicated by the dashed lines.

$\sqrt{s_{NN}} = 2.7, 3.3, 4.3, 4.9, 6.3, 7.6, 12$ GeV justifies the usage of the present model. Quantitatively, we found that the χ^2/dof improvement for the SFO+ γ_s model is $\chi^2/dof=1.5/14$, i.e. even better than it was achieved in [7] with $\chi^2/dof=3.3/14$ for the γ_s fitting approach and with $\chi^2/dof=6.3/14$ for the SFO model with $\gamma_s = 1$.

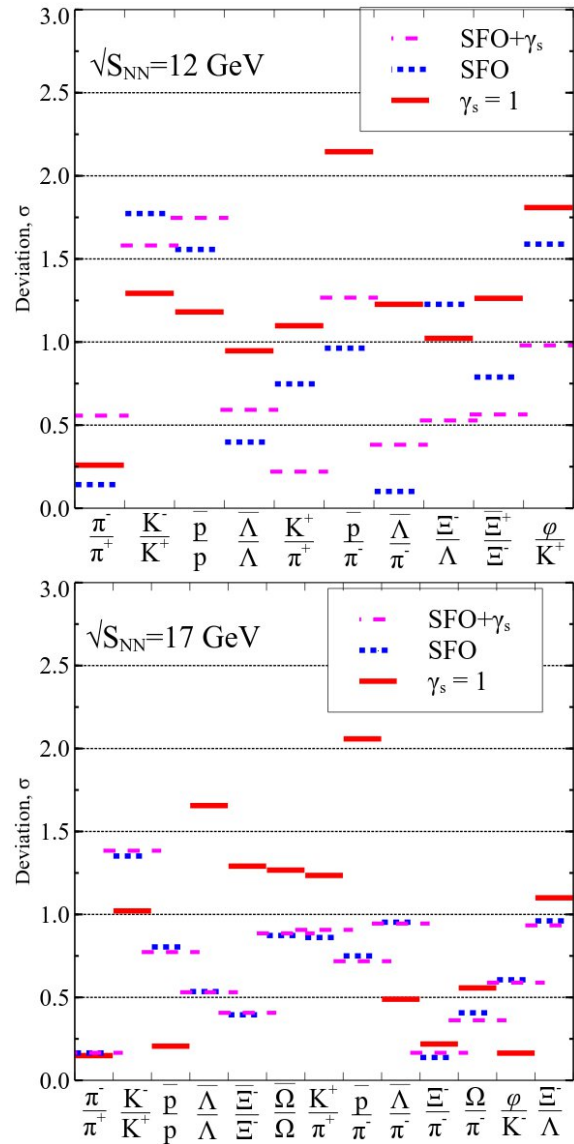


Fig. 7. (Colour on-line) Same as in Fig. 6, but for $\sqrt{s_{NN}} = 12$ and 17 GeV.

From Fig. 9 one can see that at two highest RHIC energies the description of ratios within the single FO model is very good for all ratios except for $\bar{\Lambda}/\pi^-$ at $\sqrt{s_{NN}} = 130$ GeV and for $(\Omega + \bar{\Omega})/\Xi^-$ at $\sqrt{s_{NN}} = 200$ GeV. The main reason is that at these energies all chemical potentials except for the strange one are almost zero and hence the number of particles and antiparticles is almost the same. As one can see from the upper panel of Fig. 9, the SFO+ γ_s fit significantly improves only the Ω/π^- and Ξ^-/π^- ratios compared to the single FO model, i.e. only two ratios of strange hadrons

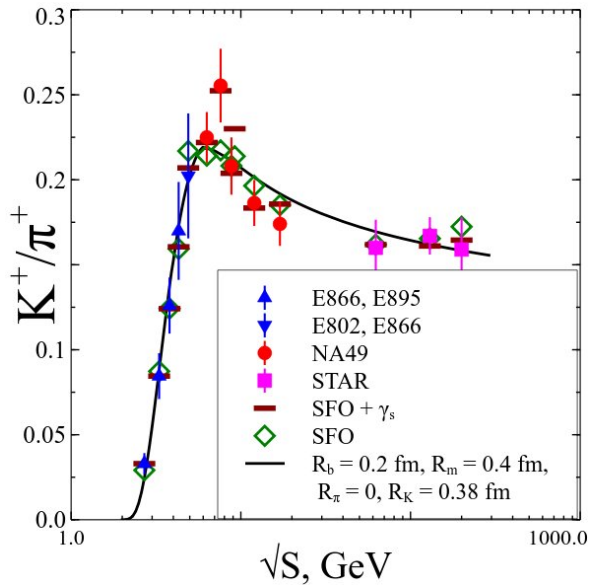


Fig. 8. (Colour on-line) $\sqrt{s_{NN}}$ dependences of K^+/π^+ ratio. The solid line corresponds to the results of [5]. Horizontal bars correspond to the present model with SFO+ γ_s fit, while the diamonds correspond to the results previously obtained for SFO [7].

responded to the variation of two additional parameters. For $\sqrt{s_{NN}} = 200$ GeV the SFO+ γ_s fit significantly improves only the $(\Omega + \bar{\Omega})/\Xi^-$ ratio and worsens the Λ/π^- ratio and ϕ/p (less), i.e. only three ratios of strange hadrons responded to such a sophisticated fit. For $\sqrt{s_{NN}} = 62.4$ GeV only two ratios out of five include kaons and, hence, using T_{SFO} and γ_s one can perfectly reproduce the strange particle ratios without affecting the non-strange ones. Treating the T_{SFO} values found within the SFO model as an additional datum for the SFO+ γ_s fit, we obtain the same result. Therefore, in contrast to low collision energies at high collision energies only a few ratios with strange particles can be improved by simultaneous variation of T_{SFO} and γ_s and, hence, the SFO cannot represent the majority of fitted ratios which are well reproduced even within the single FO model with a single or with several hard-core radii. The lower panel of Fig. 5 evidently supports such a conclusion for the HRGM with the same value of hadronic hard-core radius.

Within the SFO+ γ_s model the Λ/π^- and $\bar{\Lambda}/\pi^-$ ratios demonstrate some worsening compared to less sophisticated models. In Fig. 10 we show that the SFO+ γ_s model still does not improve these ratios. The Λ/π^- fit quality, for instance, is $\chi^2/dof=10/8$. Hence, up to now the best fit of the Λ/π^- ratio was obtained within the SFO approach with $\gamma_s = 1$. As it was mentioned

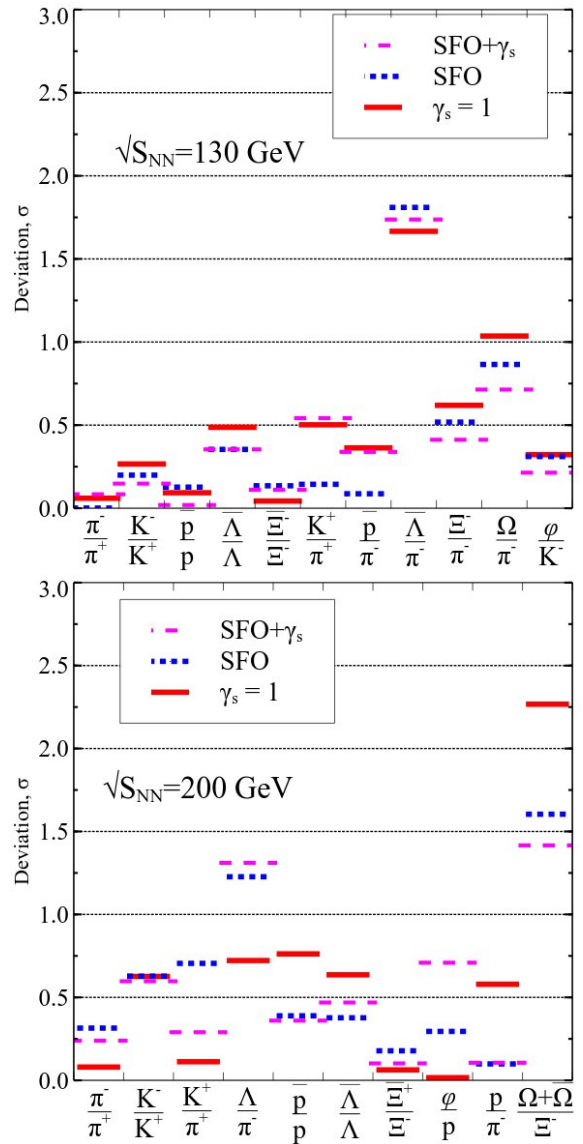


Fig. 9. (Colour on-line) Same as in Fig. 6, but for $\sqrt{s_{NN}} = 130$ and 200 GeV.

in [1, 3, 5] a too slow decrease of model results for Λ/π^- ratio compared to the experimental data is typical for almost all statistical models. Evidently, the too steep rise in Λ/π^- behavior is a consequence of the $\bar{\Lambda}$ anomaly [1, 37]. Similar results are reported in Refs. [38–40] as the \bar{p} , $\bar{\Lambda}$ and $\bar{\Xi}$ selective suppression. Since even an introduction of the separate strangeness freeze-out with the strangeness enhancement factor does not allow us to better describe these ratios, we believe that there is a corresponding physical reason which is responsible for it. One of them could be a necessity to introduce the

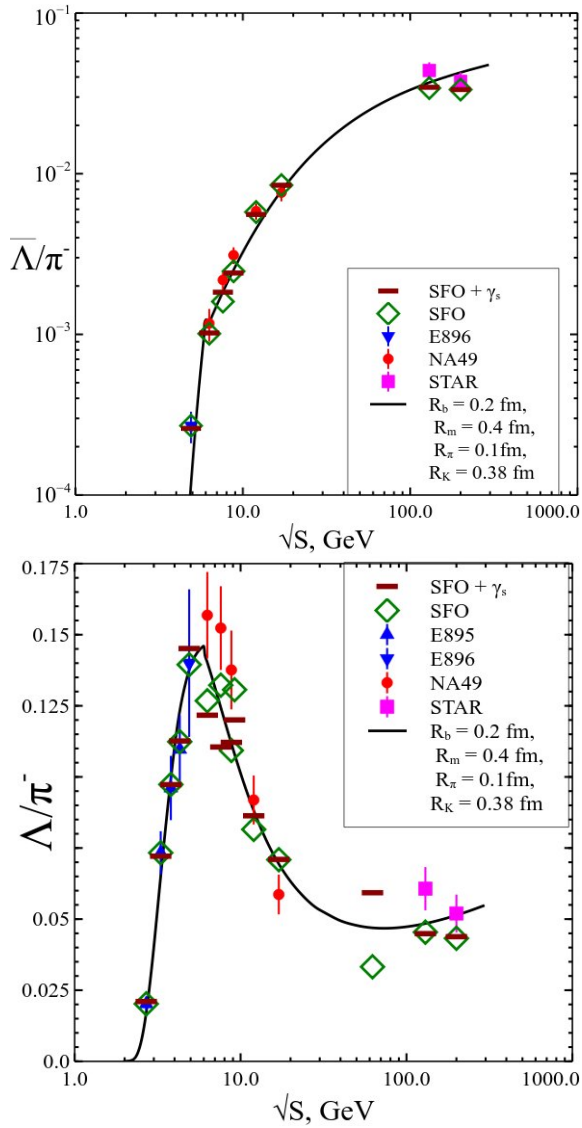


Fig. 10. (Colour on-line) $\sqrt{s_{NN}}$ dependences of $\bar{\Lambda}/\pi^-$ (upper panel) and Λ/π^- (lower panel) ratios. The solid line correspond to the results of a single FO model [5]. Horizontal bars correspond to SFO+ γ_s model, while the diamonds correspond to the previously obtained results for the SFO model [7].

different hard-core radius R_Λ for the Λ (anti)hyperons [12].

6. Conclusions

We present a thorough investigation of the data measured at AGS, SPS and RHIC energies within different versions of the multi-component hadron resonance gas model. The suggested approach to separately treat

the freeze-outs of strange and non-strange hadrons with the simultaneous γ_s fitting gives rise for the top-notch Strangeness Horn description with $\chi^2/dof=1.5/14$. The developed model clearly demonstrates that the successful fit of hadronic multiplicities includes all the advantages of these two approaches discussed in [7]. As a result for $\sqrt{s_{NN}} = 6.3, 7.6, 12, 130$ GeV we found a significant data fit quality improvement.

At the same time the lack of available data at $\sqrt{s_{NN}} = 2.7, 3.3, 3.8, 4.3, 9.2, 62.4$ GeV forced us to redefine the fitting procedure at these collision energies in order to avoid the mathematical inconsistency which in combination with the large experimental error bars led to rather large uncertainties of the fitting parameters. The suggested redefinition of the fitting procedure by including the T_{SFO} temperatures obtained for these energies within the SFO model allowed us to avoid the mathematical problems and to get the safe answers on the values of the residual chemical non-equilibrium of strange particles. The developed sophisticated HRGM, i.e. the SFO+ γ_s model, allowed us to describe the hadron multiplicity ratios with rather high quality $\chi^2/dof = 43.72/47 \simeq 0.93$. This very fact demonstrates that the suggested approach is a precise tool to elucidate the thermodynamics properties of hadron matter at two chemical freeze-outs. The fresh illustrations to this statement can be found in [14].

The achieved total value of $\chi^2 = 43.72$ for the SFO+ γ_s model is almost 50% lower than the χ^2 value found for the single FO model and 30% lower than the SFO model χ^2 value. The obtained γ_s values are consistent with the conclusion $\gamma_s \simeq 1$ (within the error bars). An evident exception is the topmost point of the Strangeness Horn (located at $\sqrt{s_{NN}} = 7.6$ GeV), at which the mean value of the strangeness enhancement factor is $\gamma_s \simeq 1.19 \pm 0.15$. To reveal the physical reason for such a deviation we need more experimental data with an essentially higher accuracy.

One of the main results obtained here is that the idea of separate chemical FO of strange hadrons provides a very high quality of the data description. Further inclusion of the chemical non-equilibrium on top of the SFO is consistent with the result $\gamma_s \simeq 1$ for all energies except for $\sqrt{s_{NN}} = 7.6$ GeV. Thus, the found residual chemical non-equilibrium of strange particles is weak and, hence, it can be safely ignored for all energies except for $\sqrt{s_{NN}} = 7.6$ GeV. The strange charge enhancement of about 20% found at this collision energy allowed us to perfectly describe the topmost point of the Strangeness Horn, but at the expense of the worsening of Λ/π^- and $\bar{\Lambda}/\pi^-$ ratios.

In addition, the description of ratios containing the non-strange particles, especially such as π^-/π^+ and \bar{p}/p , gets better compared to previously reported results [5,7]. The remaining problem of the ratios involving the Λ and Ξ (anti)hyperons can be resolved by an inclusion of the different hard-core radius for Λ (anti)particles [12], but such a treatment is out of scope of the present work.

The performed analysis of the SFO+ γ_s model hadronic pressures existing at FO and at SFO allowed us to elucidate an important conclusion that the single FO models with the same hard-core radius [1] or with different hard-core radii [4, 5, 7] for all hadrons reproduce the SFO pressure for all collision energies below $\sqrt{s_{NN}} = 62.4$ GeV. The main reason for such a behavior is that the number of ratios involving strange hadrons is larger than the number of ratios with non-strange hadrons.

Also we report an existence of strong jumps in the SFO pressure, the SFO temperature and the corresponding effective number of degrees of freedom, when the center of mass collision energy changes from 4.3 to 4.9 GeV. Based on the concept of non-smooth chemical freeze-out introduced recently in [14], we parameterized the dependencies $T_{FO}(\sqrt{s_{NN}})$ and $T_{SFO}(\sqrt{s_{NN}})$ which can be verified in the future experiments planned at FAIR (GSI) and NICA (JINR). We hope that the high precision data measured in these experiments will allow us to finally answer the question whether the residual non-equilibrium of strange charge is necessary to describe the topmost point of the Strangeness Horn or the concept of two separate chemical freeze-out for strange and non-strange hadrons can do this without introducing the γ_s factor.

Acknowledgments. We would like to thank A. Andronic for providing an access to well-structured experimental data. The authors are thankful to I. N. Mishustin, D. H. Rischke and L. M. Satarov for valuable comments. K.A.B., A.I.I. and G.M.Z. acknowledge a support of the Fundamental Research State Fund of Ukraine, Project No F58/04. K.A.B. acknowledges also a partial support provided by the Helmholtz International Center for FAIR within the framework of the LOEWE program launched by the State of Hesse.

1. A. Andronic, P. Braun-Munzinger and J. Stachel, Nucl. Phys. A **772**, 167 (2006) and references therein.
2. J. Rafelski, Phys. Lett. B **62**, 333 (1991).
3. A. Andronic, P. Braun-Munzinger and J. Stachel, Phys. Lett. B **673**, 142 (2009) and references therein.

4. D.R. Oliinychenko, K.A. Bugaev and A.S. Sorin, Ukr. J. Phys. **58**, 211 (2013).
5. K.A. Bugaev, D.R. Oliinychenko, A.S. Sorin and G.M. Zinovjev, Eur. Phys. J. A **49**, 30 (2013) and references therein.
6. K. A. Bugaev, D. R. Oliinychenko and A. S. Sorin, Ukr. J. Phys. **58**, 939 (2013).
7. K.A. Bugaev *et al.*, Europhys. Lett. **104**, 22002 (2013).
8. S. Chatterjee, R. M. Godbole and S. Gupta, Phys. Lett. B **727**, 554 (2013).
9. D. R. Oliinychenko, V. V. Sagun, A. I. Ivanytskyi and K. A. Bugaev, Ukr. J. Phys. **59**, 1051 (2014).
10. G. Zeeb, K. A. Bugaev, P. T. Reuter and H. Stöcker, Ukr. J. Phys. **53**, 279 (2008).
11. F. Becattini, J. Manninen and M. Gazdzicki, Phys. Rev. C **73**, 044905 (2006).
12. V. V. Sagun, Ukr. J. Phys. **59**, 755 (2014) .
13. S. Chatterjee *et al.*, Adv. High Energy Phys. **2015**, 349013 (2015).
14. K.A. Bugaev *et al.*, Ukr. J. Phys. **60**, 181 (2015).
15. S. Wheaton, J. Cleymans and M. Hauer, Comput. Phys. Commun. **180**, 84 (2009).
16. J. L. Klay *et al.*, Phys. Rev. C **68**, 054905 (2003).
17. L. Ahle *et al.*, Phys. Lett. B **476**, 1 (2000).
18. B.B. Back *et al.*, Phys. Rev. Lett. **86**, 1970 (2001).
19. J.L. Klay *et al.*, Phys. Rev. Lett. **88**, 102301 (2002).
20. C. Pinkenburg *et al.*, Nucl. Phys. A **698**, 495c (2002).
21. S. Albergo *et al.*, Phys. Rev. Lett. **88**, 062301 (2002).
22. P. Chung *et al.*, Phys. Rev. Lett. **91**, 202301 (2003).
23. S.V. Afanasiev *et al.*, Phys. Rev. C **66**, 054902 (2002).
24. S.V. Afanasiev *et al.*, Phys. Rev. C **69**, 024902 (2004).
25. T. Anticic *et al.*, Phys. Rev. Lett. **93**, 022302 (2004).
26. S.V. Afanasiev *et al.*, Phys. Lett. B **538**, 275 (2002).
27. C. Alt *et al.*, Phys. Rev. Lett. **94**, 192301 (2005).
28. S.V. Afanasiev *et al.*, Phys. Lett. B **491**, 59 (2000).
29. B. Abelev *et al.*, Phys. Rev. C **81**, 024911 (2010).
30. B. Abelev *et al.*, Phys. Rev. C **79**, 034909 (2009).
31. J. Adams *et al.*, Phys. Rev. Lett. **92**, 182301 (2004).
32. J. Adams *et al.*, Phys. Lett. B **567**, 167 (2003).
33. C. Adler *et al.*, Phys. Rev. C **65**, 041901(R) (2002).
34. J. Adams *et al.*, Phys. Rev. Lett. **92**, 112301 (2004).
35. J. Adams *et al.*, Phys. Lett. B **612**, (2005) 181.
36. A. Billmeier *et al.*, J. Phys. G **30**, S363 (2004).
37. B. B. Back *et al.*, Phys. Rev. Lett. **87**, 242301 (2001).
38. F. Becattini *et al.*, Phys. Rev. C **85**, 044921 (2012).
39. F. Becattini *et al.*, Phys. Rev. Lett. **111**, 082302 (2013).

-
40. J. Stachel, A. Andronic, P. Braun-Munzinger and K. Redlich, arXiv:1311.4662 [nucl-th].
41. K. A. Bugaev *et al.*, Phys. Part. Nucl. Lett. **12**, 238 (2015).